Digital in-line holography with photons and electrons

2001 J. Phys.: Condens. Matter 13 10729

(http://iopscience.iop.org/0953-8984/13/47/313)

INSTITUTE OF PHYSICS PUBLISHING JOURNAL OF PHYSICS: CONDENSED MATTER

J. Phys.: Condens. Matter **13** (2001) 10729–10741 PII: S0953-8984(01)25649-5

Digital in-line holography with photons and electrons

H J Kreuzer[1], **M J Jericho**[1], **I A Meinertzhagen**[2] **and Wenbo Xu**[1,2]

[1] Department of Physics, Dalhousie University, Halifax, N.S. B3H 3J5, Canada
[2] Neuroscience Institute and Department of Psychology, Dalhousie University, Halifax, N.S. B3H 3J5, Canada

Received 11 June 2001
Published 9 November 2001
Online at stacks.iop.org/JPhysCM/13/10729

Abstract

We review the status of digital in-line holography with numerical reconstruction. Its application in optics with a laser as a source of coherent radiation has been perfected in recent years with optimal resolution achievable on a routine basis in such diverse areas as three-dimensional mapping and tracking of micron-sized particle distributions, growth of polymer spherulite, and structural studies of cells and micro-organisms. Digital in-line holography with coherent low-energy electron beams from an atomic-sized field emitter tip has now achieved nanoscale resolution and can, according to theoretical simulations and estimates, achieve atomic resolution, one hopes in the near future.

(Some figures in this article are in colour only in the electronic version)

1. Introduction

Over 50 years ago, Gabor [1] proposed a new principle of microscopy to overcome the limitations of lenses. Using a coherent ensemble of particles with wave nature, the fraction of the beam elastically scattered by an object is made to interfere with a coherent reference wave at a two-dimensional detector creating a hologram that contains information on both the amplitude and the phase of the scattered wave. In-line holography with spherical waves, as originally proposed by Gabor, is the simplest realization of the holographic method, working without lenses. Its applications have been limited, however, until recently due to the fact that reconstruction of the object image with another wave (light or electrons) is not practical. To avoid this problem, various schemes of off-line holography have been developed [2–4]. Another option, which was also suggested in the early days of holography, is numerical reconstruction [5–10]. Most of these approaches were unsatisfactory because of poor image quality due to approximations in the reconstruction algorithm. A recently designed reconstruction algorithm overcomes these shortcomings and yields reconstructed images of the highest resolution [11, 12]. Although this scheme was originally proposed for in-line holography with electrons, its transfer to optical holography is straightforward [13–19].

In in-line holography a spherical wave of wavelength λ, emanating from a 'point' source of linear dimensions of the order of the wavelength, illuminates an object, typically a distance of a few thousand wavelengths from the source, and forms a highly magnified diffraction pattern on a screen much further away; see figure 1. We denote by $A(\boldsymbol{r}, t)$ the wave amplitude (the wave function for electrons or the electric field vector for photons) and split it into the unscattered reference wave, $A_{ref}(\boldsymbol{r}, t)$, and the wave, $A_{scat}(\boldsymbol{r}, t)$, scattered by the object. Ideally the reference wave emanating from the source is a spherical wave, $A_{ref}(\boldsymbol{r}, t) = \exp(\mathrm{i}kr)/r$ where $k = 2\pi/\lambda$ is the wavenumber. In an experiment this spherical wave is modified by the emission cone of the source. However, this can be accounted for by constructing, from the intensity, $|A(\boldsymbol{r}, t)|^2$, the contrast image

$$\widetilde{I}(\boldsymbol{r}) = |A_{ref}(\boldsymbol{r}, t) + A_{scat}(\boldsymbol{r}, t)|^2 - |A_{ref}(\boldsymbol{r}, t)|^2 \tag{1}$$

$$= [A^*_{ref}(\boldsymbol{r}, t)A_{scat}(\boldsymbol{r}, t) + A_{ref}(\boldsymbol{r}, t)A^*_{scat}(\boldsymbol{r}, t)] + |A_{scat}(\boldsymbol{r}, t)|^2 \tag{2}$$

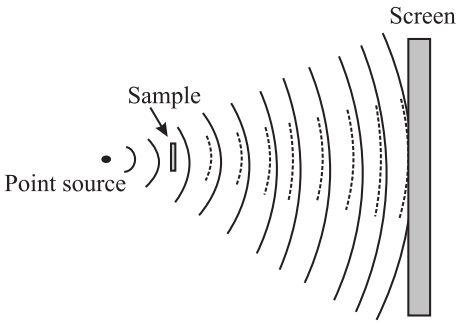

Figure 1. A schematic diagram of in-line holography: a coherent wave of radiation emanating from the point source partially scatters off an object creating a highly magnified hologram on a screen.

We will refer to the first term (in brackets) in (2), linear in the scattered wave, as the 'holographic diffraction pattern' because it arises from the superposition of the interference terms between the unscattered reference wave from the source and the scattered wave from the object. The second term in (2) contains the interference between the scattered waves. We will refer to it as the 'classical diffraction pattern'. Neither term, holographic or classical diffraction, is meant to be exclusive but simply is coined to refer to the terms in (2) linear and quadratic in the scattered waves. Holographic diffraction dominates the images for small objects; loosely speaking, 'small' means that the object should only block a fraction of the cone of radiation recorded on the screen. Even if these objects are opaque, we are still in the regime of holography, and will be able to recover the outline or shape of the object by reconstruction. As the scattered wave amplitude grows because more of the incoming reference wave is blocked out by larger objects, classical diffraction becomes more important. When it eventually dominates the image, we are in the regime of classical wave optics where image formation can then be described as diffraction around macroscopic objects. Diffraction around an opaque object or diffraction at the rim of a hole in an opaque target also requires interference between the reference and scattered waves, i.e. is described by the first term in (2). Indeed, one can apply the holographic reconstruction algorithm, given below to obtain the shape of the opaque object (or hole) as we have shown elsewhere [14].

Holography is a two-step process: first, a hologram must be recorded, and second, reconstruction must yield an 'image' of the object, i.e. the intensity of the wavefront at the object. In digital in-line holography—DIH—the hologram is recorded by a detector array,

such as a multichannel plate for electrons or a CCD camera for photons, and transferred to a computer in which the reconstruction is done numerically. The role of reconstruction is to obtain the three-dimensional structure of the object from the two-dimensional hologram on the screen, or, in physical terms, to reconstruct the wavefront at the object. This can be achieved via a Kirchhoff–Helmholtz transform[1] [11]

$$K(\boldsymbol{r}) = \int_S \mathrm{d}^2\xi \; \widetilde{I}(\boldsymbol{\xi}) \exp\left[2\pi \mathrm{i}\boldsymbol{\xi}\cdot\boldsymbol{r}/(\lambda\xi)\right] \tag{3}$$

in which the integration extends over the two–dimensional surface of the screen with coordinates $\boldsymbol{\xi} = (X, Y, L)$ where L is the distance from the source (pinhole) to the centre of the screen (CCD chip); and $\widetilde{I}(\boldsymbol{\xi})$ is the contrast image (hologram) on the screen obtained by subtracting from the image with the object present that without the object present. The function $K(\boldsymbol{r})$ is significantly structured and different from zero only in the space region occupied by the object. By reconstructing the wavefront $K(\boldsymbol{r})$ on a number of planes at various distances from the source in the vicinity of the object, a three-dimensional image can be built up from a single two-dimensional hologram. $K(\boldsymbol{r})$ is a complex function and one usually plots its magnitude to represent the object, although phase images are also available. For the numerical implementation of the transformation we have developed a fast algorithm that evaluates $K(\boldsymbol{r})$ without any approximations. It is incorporated in a self-contained program package, originally developed for electron holography, called LEEPS, that performs not only the numerical reconstruction but also all other procedures connected with data management and visualization [12].

In holography, the term 'reconstruction' is used to obtain the function $K(\boldsymbol{r})$ from the hologram. The plot of $|K(\boldsymbol{r})|$ on a two-dimensional plane, which we will call a 2D holographic reconstruction, perpendicular to the optical axis is equivalent to one in-focus image taken in a conventional compound microscope. In DIH one can generate a stack of 2D holographic reconstructions from a single hologram. Combining such a stack will result in a three-dimensional image of the object; this latter step is usually referred to as 3D reconstruction.

A frequently voiced criticism of DIH, propagated in most textbooks, is connected with the so-called twin-image problem. We recall that, due to its phase sensitivity, reconstruction gives a structured wave amplitude not only at the position of the object, d, the distance from the source to the object, but also at $-d$, i.e. the same distance on the other side of the source. If, as in photoelectron holography, the source–object distance is of atomic dimension and of the same order as the expected resolution of the method, the signal from the twin image at the location of the object is substantial causing severe distortions of the reconstructed image. Thus ingenious methods have been devised to eliminate the twin image, such as energy averaging [23]. For DIH, on the other hand, the twin image does not represent a problem. The reason is one of geometry and much akin to a similar 'solution' to the twin-image problem achieved in Fraunhofer holography [24]. If the source–object distance is, as a typical example, several thousand times the wavelength, then the twin image is the same distance on the other side of the source and the signal produced by it at the object is smeared out over the length scale of the achievable resolution for a given screen size. Thus if one chooses a screen size large enough to achieve a resolution of the order of the wavelength, the background signal introduced by the twin image is negligibly small as we have shown before and will do again in this article. Reducing the screen size will then not only reduce the resolution but will concurrently enhance the background signal, leading to artificial structures in the reconstructed image that may be

[1] The use of the Kirchhoff–Helmholtz transform for reconstruction was already proposed by Gabor [20], it was also used by Barton [21] and others for the reconstruction of photoelectron holograms, and in LEED holography [22]; see other articles in this Special Issue. It was then applied in LEEPS (low-energy electron point source) microscopy and used subsequently in optical in-line holography as we will document further below.

interpreted as the twin image. We hasten to add that the same deterioration will take place if uncontrolled approximations are made in the reconstruction formula (3) such as an on-axis approximation amounting to setting in the denominator of the argument of the exponential function $\xi = (X^2+Y^2+L^2)^{1/2} \simeq L$. To summarize: the twin image is not a problem in DIH in that it can be reduced to below the noise level by using a large enough recording screen (for an object of a given size) such that, in principle, one achieves the desired resolution (of the order of the wavelength). At the same time, it is mandatory that one uses the Kirchhoff–Helmholtz reconstruction formalism without approximations.

This paper is structured as follows. In the next section we will begin with optical DIH where the ultimate goal of holography, namely to obtain three-dimensional images of an object with the resolution of the order of the wavelength, is now routinely achieved. In the course of pursuing this work, DIH has been developed into a new tool in such diverse areas as cell biology, microparticle imaging and tracking, and polymer crystallization. In section 3 we will review recent progress in LEEPS microscopy and discuss some of the still outstanding problems to be addressed in the near future.

2. Optical DIH

2.1. Experimental set-up

The experimental set-up for optical DIH, following the schematic diagram of figure 1, is very simple: a laser is directed onto a pinhole, of diameter of the order of the wavelength, which acts as the 'point source' from which a spherical wave, of wavelength λ, emanates. The wave illuminates an object, in our set-up a few millimetres from the pinhole, and forms a geometrically magnified diffraction pattern on a screen, in our case a CCD chip, a few centimetres away. If the scattered wave, shown by the dotted lines in figure 1, from the object is small compared with the unscattered reference wave, the interference pattern on the screen constitutes a hologram, linear in the scattered wave. The hologram is stored as a digital image in a computer for reconstruction.

To establish DIH as a new microscopy it is important to make detailed comparisons between images from conventional compound light microscopy and those obtained with DIH. For this purpose we used a standard inverted compound microscope (Zeiss Axiovert 25) and obtained a digital record of the bright-field image seen through the eyepiece in the normal way. To record a hologram of the same sample area, a pinhole (typical diameter 1–5 μm) was placed between the objective lens and the sample such that the spherical light waves from the pinhole passed through the selected sample area. The laser light that illuminated the pinhole was introduced through a side port in the microscope and was directed towards the objective lens and pinhole via a movable mirror. The hologram was recorded with a CCD camera (1020×1532 pixels, pixel size 9 μm square) that was supported on the microscope work plate and centred over the pinhole and the selected area of the sample. The distance of the CCD camera from the pinhole, typically a few centimetres, was adjusted to capture all interference fringes of the hologram that could be resolved with enough pixels. The pinhole was mounted on an X–Y micrometer stage and could be moved out of the way to image the sample in the bright field. This arrangement of the equipment minimized vibrations and also provided an easy method for switching from bright-field to holographic modes of operation.

The object of lateral dimension a to be visualized was placed a distance d, typically a few millimetres, from the pinhole such that the Fraunhofer condition, $a^2 \ll d\lambda$, was fulfilled, in order to guarantee (i) that the image on the screen was dominated by its holographic part, and (ii) that twin-image effects in the reconstruction were minimized.

The resolution in the reconstructed images depends on the information recorded in the hologram which, in turn, is limited by the size of the recording CCD chip and its resolution. For a digitally recorded hologram this is given by the number of pixels, their size and spacing, and the dynamic range of the recorded signals.

From diffraction theory we know that the resolution of an optical system is given by $a = 0.61\lambda/\sin\vartheta$, where ϑ is half the opening angle of the divergent beam illuminating the object. To achieve this resolution we thus need a recording screen of diameter D at a distance L from the source such that $D/2L > 1/\sqrt{(a/0.61\lambda)^2 - 1}$. This also follows from inspection of the reconstruction formula which suggests that two points separated in the object by a distance a will be resolved if their contribution to the interference pattern at the edge of the screen is out of phase, i.e. we have $k\boldsymbol{\xi}\cdot(\boldsymbol{r}+\boldsymbol{a})/\xi - k\boldsymbol{\xi}\cdot\boldsymbol{r}/\xi > 2\pi$. The number of pixels and the dynamics of the CCD chip used for recording the hologram must, of course, resolve the closest diffraction fringes.

As we mentioned above, the input to the reconstruction formula (3) is the *contrast* image for a perfectly spherical incoming wave. It transpires that perfecting this image is the hardest part in the practical implementation of DIH. Guided by the experience in photoelectron and LEED holography [22] we have implemented the following procedure:

(i) Record digitally the hologram of the object, giving a matrix I_{nm} of the intensity recorded on the CCD chip, where n and m enumerate the pixels in the x- and y-directions.
(ii) Remove the object and record digitally the intensity matrix $I^{(0)}_{nm}$ of the illuminating laser.
(iii) Construct numerically the contrast image, corrected for the intensity variations in the primary laser beam:

$$\widetilde{I}_{nm} = (I_{nm} - I^{(0)}_{nm})/\sqrt{I^{(0)}_{nm}}. \tag{4}$$

By this procedure almost all imperfections in the laser source are eliminated. Indeed, this step minimizes the quality requirements on the laser itself, as long as the laser is sufficiently stable to capture identically both images. We have checked this by comparing the contrast images obtained with (i) a high-quality laser and (ii) a cheap laser pointer. The results in reconstruction are of comparable quality.

The contrast image is next used in the reconstruction algorithm, based on the transform (3), to produce a series of 2D holographic reconstructions at different distances from the source, i.e. the pinhole. Because the source–object distance can be measured directly with an accuracy of only a millimetre or so, it is necessary to zoom in with a series of reconstructions at different distances, displayed in the LEEPS program package as a film, to achieve accuracy at the micron level.

2.2. Examples of optical DIH

To demonstrate the state of the art in optical DIH we show in figure 2 holograms and images of latex microspheres having a mean diameter of 1 μm. The spheres (refractive index 1.59 at 589 nm) were mounted in a thin layer of gelatin between a microscope slide and a glass cover slip. A hologram, i.e. the intensity matrix I_{nm} taken with a blue laser, is shown in panel A. To obtain the intensity matrix of the light source, $I^{(0)}_{nm}$, the slide was moved sideways to an area that contained only gelatin but no spheres. This reference hologram (panel C) was subtracted from the hologram in panel A to obtain the contrast hologram, panel E.

In panel B we show a 2D holographic reconstruction from the original, uncorrected hologram of panel A, taken through the equatorial plane of the spheres. The image clearly resolved all spheres but also shows a substantial noise level. Starting, on the other hand, from

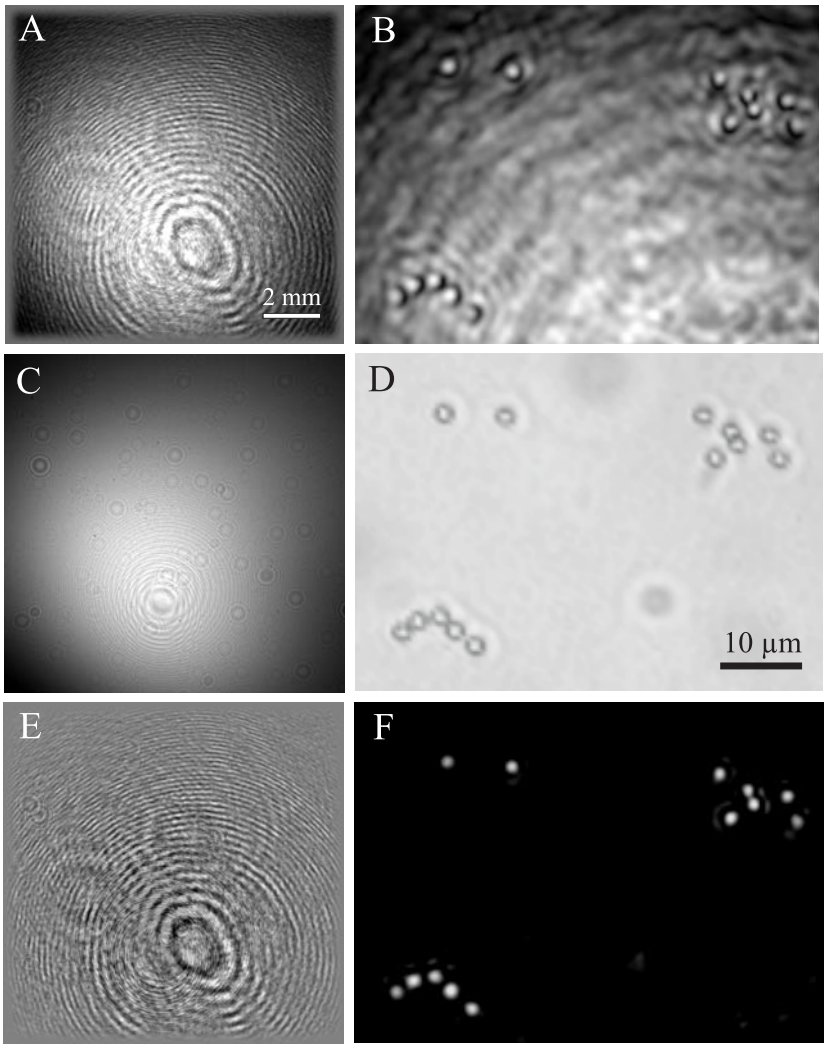

Figure 2. Latex microspheres (1.09 μm diameter) embedded in gelatin between glass plates. A: a hologram (1024 $\times$ 1024 pixels). B: the reconstruction from A through the equatorial plane of the spheres. C: the intensity distribution of the laser radiation with the object removed. D: the bright-field image obtained with the compound light microscope (Zeiss Plan-Neofluar 40$\times$/0.75 objective). E: the contrast hologram obtained by subtracting C from A. F: the 2D reconstruction from the contrast hologram E. Blue laser; 1 μm pinhole. Pinhole–sample distance 2.3 mm; pinhole–CCD chip distance 1.75 cm.

the contrast hologram, panel E, gives a perfect reconstruction, panel F. Indeed, this image is better than the bright-field image in panel D taken with the compound microscope for which diffraction rings already show up. Also note that there is *no* twin image at all.

As an aside we should briefly comment on the intensities in these pictures. In a bright-field image of a compound microscope, transparent spheres are bright and opaque spheres are dark, both on a light background. In contrast, the background in the holographic reconstruction is dark because we used a contrast hologram from which the bright background is subtracted. Any objects, transparent or opaque, are lighter than the background because both are the origins

of scattered waves which we have traced back from the hologram in the reconstruction. After all, the contrast image (4) from which the reconstruction is done is identically zero in the absence of an object, leading to a uniformly black reconstructed image. Because an opaque sphere absorbs more of the incoming light, it is less bright than a transparent sphere.

The power of DIH is that image information is not limited to a plane but is truly three-dimensional. 2D holographic reconstructions can thus be performed from a single hologram at a series of selected object depths and the 3D reconstruction of the object can be generated from such a stack of 2D reconstructions. We have done this for 5 μm latex spheres; see figure 3. Panel A shows a bright-field image with the compound microscope and panel B shows a 2D holographic reconstruction on the plane, perpendicular to the optical axis, of maximum intensity contrast, i.e. the plane where the spheres are. Panel C shows the spheres in a 3D reconstruction, viewed as if along the optical axis, that was obtained from a stack of 15 consecutive 2D hologram reconstructions. That a single hologram, in this case the one leading to the reconstruction in panel B, contains the full three-dimensional structure of the spheres is illustrated in panel D, in which the same stack of 15 reconstructed sections was viewed as if along one axis of the section plane, to provide a side view of the spheres. Viewed from this direction, all spheres lie nearly in the same plane (as the sample geometry requires) and the spheres have again circular profiles. The two spheres that were in contact appear to occupy slightly different positions perpendicular to the sample plane.

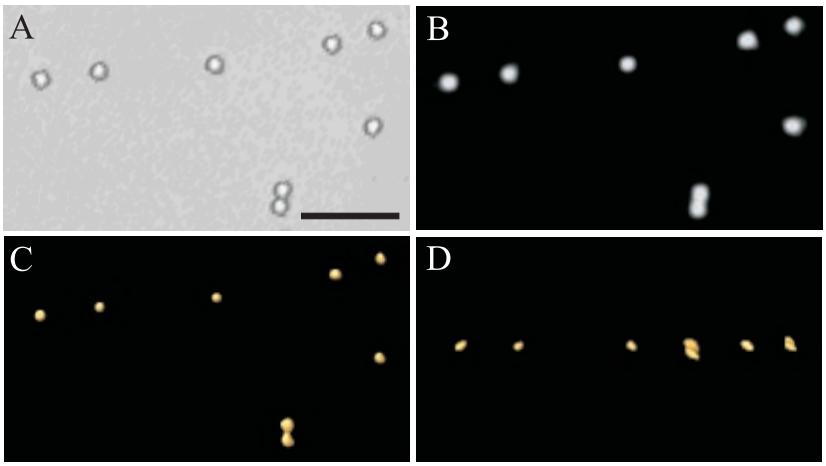

Figure 3. 5.13 μm polymer microspheres mounted in gelatin. A: a bright-field compound microscope image (Zeiss 25×/0.80 Plan-Neofluar objective). B: the holographic 2D reconstruction in a plane corresponding to A. C, D: the 3D reconstruction from 15 2D holographic reconstructions (of which panel D is number 8), using a software package (Amira: Konrad Zuse Centrum, Berlin): (C) viewed along the optical axis, and (D) viewed from the side. Pinhole–object distance 1.5 mm; pinhole–CCD chip distance 4.8 cm; green laser ($A = 532$ nm); 2 μm pinhole.

To demonstrate the effect of the screen size, i.e. the amount of information used in reconstruction, we show in figure 4 results for a mixture of transparent latex spheres and opaque Fe_3O_4 beads of diameters 5 and 4 μm, respectively, with a bright-field image from a compound microscope in panel A. Panel B shows the contrast hologram, as obtained with a 2D reconstruction shown in panel C. The holograms in panels D and F were obtained from the hologram of panel B by cutting out the central quarter and sixteenth sections, respectively. As a result of reducing the amount of information now used in the reconstruction, the 2D reconstruction in panel E is less clear and that in panel G lacks resolution with a substantial

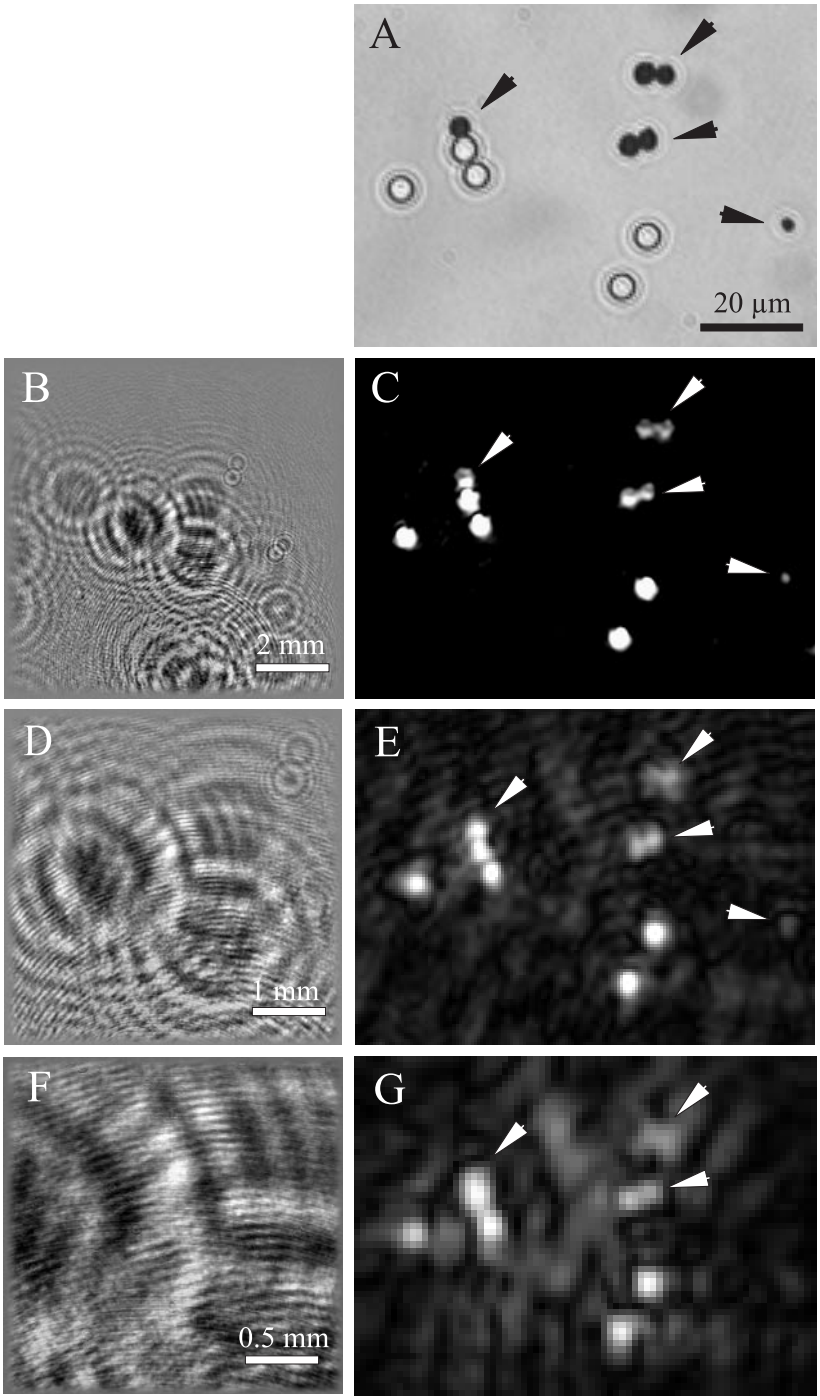

Figure 4. 5.13 μm transparent latex spheres and 4.5 μm opaque Fe_3O_4 beads (arrows) embedded in gelatin. A: a bright-field compound microscope image (Zeiss 40×/0.75 Plan-Neofluar objective). B: the hologram with 1024 × 1024 pixels on an area of 0.92 cm × 0.92 cm. C: the holographic 2D reconstruction in a plane corresponding to A. D: the centre section of the hologram in B with only 512 × 512 pixels on an area of 0.46 cm × 0.46 cm. E: the reconstruction from D. F: the centre section of the hologram in D with only 256 × 256 pixels on an area of 0.23 cm × 0.23 cm.

background noise appearing. The latter could be attributed to the twin image but our point is that with proper care exercised in setting up the DIH geometry any such undesired features in the reconstruction, be they from the twin image or not, can be reduced below a tolerable noise level.

DIH has by now been developed into a new microscopy in biology [19]. As an example, we show reconstructed images of a unicellular marine plant cell, the diatom *Ditylum brightwellii*, mounted unstained in gelatin (figure 5).

Images obtained using DIH (panels E and F of figure 5) are compared with those either from differential interference microscopy using a conventional compound light microscope

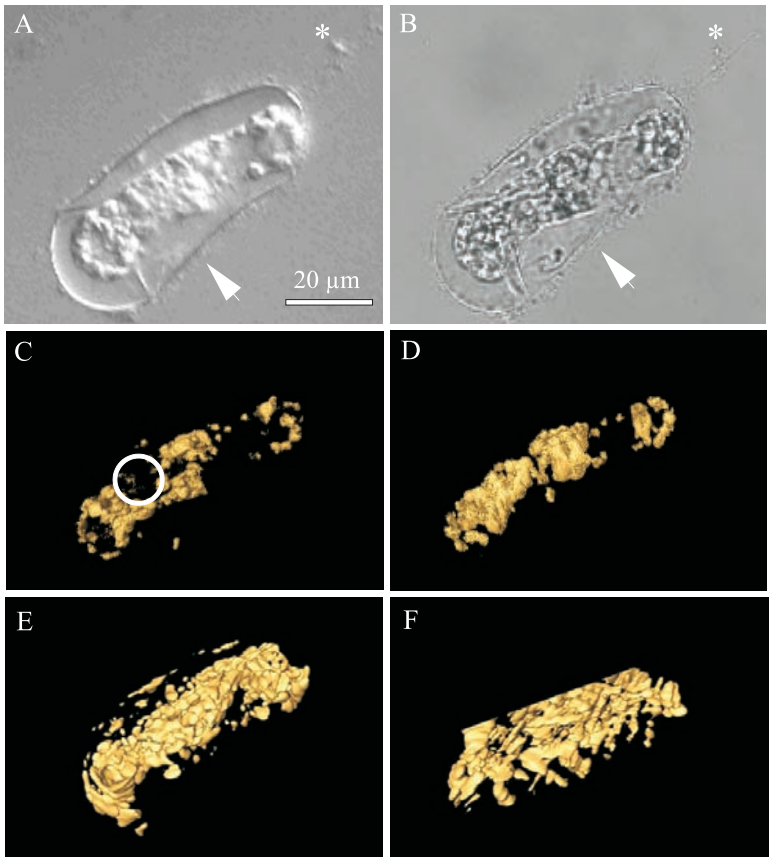

Figure 5. A single cell of *Ditylum brightwellii*. A: a differential interference microscope image obtained with a Zeiss Plan-Neofluar 40×/0.75 objective. B: a bright-field image obtained in the transmission mode of a confocal microscope with a 40×/1.30 oil objective. Note the resolution of the outer siliceous frustule (arrowhead) but poor contrast and depth resolution of the cell contents in these two images. As a fortuitous marker, a single unidentified bacterium (asterisk) in panels A, B is attached to the frustule spine (B). C, D: the 3D image stack of the signal from the specimen autofluorescence obtained by LSCM and reconstructed from 23 slices at 1 μm intervals, using the same specimen and objective as in panel B; note the contrast resolution of the cell contents and the absence of fluorescence in the region enclosed by the circle; C is viewed from the same direction as in A and B, while in D the reconstruction is rotated by 90° about the cell's long axis from the view in C. E, F: the 3D reconstruction of the corresponding DIH image stack; E shows the same view as in C, but along the optical axis, while F shows the rotated view, perpendicular to that of panel C, as in D.

(DIC) (figure 5, panel A), a bright-field transmitted-light image (figure 5, panel B), and two views of a stack of images obtained by laser scanning confocal microscopy (LSCM) and reconstructed in 3D using software (Amira: Konrad Zuse Centrum, Berlin) (panels C and D of figure 5). Note that all images are shown at the same magnification, using the same objective. Panels A and B of figure 5 are sections, whereas panels C to F are 3D reconstructions. It is clear that the fluorescence images of panels C and D of figure 5, originating mostly from the cell's chlorophyll-bearing plastids, contain only a subset of the structures imaged by DIH in panels E and F of figure 3. In particular, the frustule visible in CID microscopy (figure 5, panel A) is imaged by DIH, but does not appear in LSCM because it fails to generate a significant fluorescence signal. More complete evaluation of the DIH reconstructions can be made with reference to the original 2D DIH images representing cuts through the cell. We refer the reader to an earlier paper where further details are given [19].

DIH can also be used successfully on macroscopic biological specimens, prepared by standard histological procedures, as for a histological section of the head of the fruit fly, *Drosophila melanogaster*. Such images reveal the structure of the pigmented compound eye, and different neuropile regions of the brain within the head cuticle including the optic neuropiles underlying the compound eye [19]. Another recent application of DIH concerns the structure of polymer spherulites [25].

3. LEEPS microscopy

In-line holography with electrons was attempted experimentally for the first time in the 1950s [26] and has since then been successfully applied in transmission electron microscopy. A number of publications review the history of this field and the present status of electron holography [27–30]. Pioneering attempts in *lensless* electron projection microscopy were performed almost 60 years ago [31]. However, lensless in-line holography with low-energy electrons had to await the availability of a sufficiently coherent electron source and the technology to accurately position this source with nanometre precision. This new kind of microscopy with point sources, now called low-energy electron point source (LEEPS) microscopy, was pioneered by Fink *et al* [32], and evolved from combining the technological tools of scanning probe microscopy with new ideas in projection microscopy [33, 34]. In a LEEPS microscope an ultrathin metal tip with one or a few atoms at its apex [35–37] serves as a 'point' source[2] for a coherent electron beam with a virtual source size of atomic dimensions as determined from interferometric measurements [38] and capable of emitting currents up to milliamperes [39]. The electrons are accelerated to energies in the range of 20–200 eV and scatter off the atoms of a sample a distance $d = 0.1$–$1\ \mu$m away (see the schematic diagram in figure 1). On a screen at a distance $D \simeq 10$ cm behind the object an image is formed with a magnification of D/d. If the object only blocks a small fraction of the incoming electron beam, most of the electron wavefronts arrive on the screen unscattered and we have the typical situation of an in-line hologram.

The first holograms obtained by Fink and collaborators [32,40] were of carbon nanofibres. Later, holes in thin films were imaged and reconstructed [14], as were carbon nanotubes [41]. First images and reconstructions of macromolecules were also obtained with a resolution in the nanometre range [41–43]. As an example we show the (experimental) hologram of a

[2] The flux of electrons can be considered coherent if (1) it is sufficiently monoenergetic and (2) the virtual source size is small compared to the wavelength. The resulting coherence length must be at least as long as the maximum difference of all optical paths needed for taking the hologram. If this is experimentally realized, theory can treat such a source as a 'point' source, using the quotation marks to indicate that this is a theoretical abstraction. See also the next section for further discussion.

phthalocyaninato polysiloxane (PcPS) molecule together with a model of this rod-like polymer and its numerical reconstruction [43] (figure 6).

As numerous simulation results have shown, atomic resolution should be obtainable with electronic energies of the order of a 100 eV, i.e. at least an order of magnitude better than what has been achieved so far in the papers cited above and also by others [44,45]. Because we have shown with optical DIH that resolution of the order of the wavelength (resolving micron-sized spheres with visible light) is possible, the difficulties encountered in LEEPS microscopy must be purely technical and will no doubt be overcome in the near future.

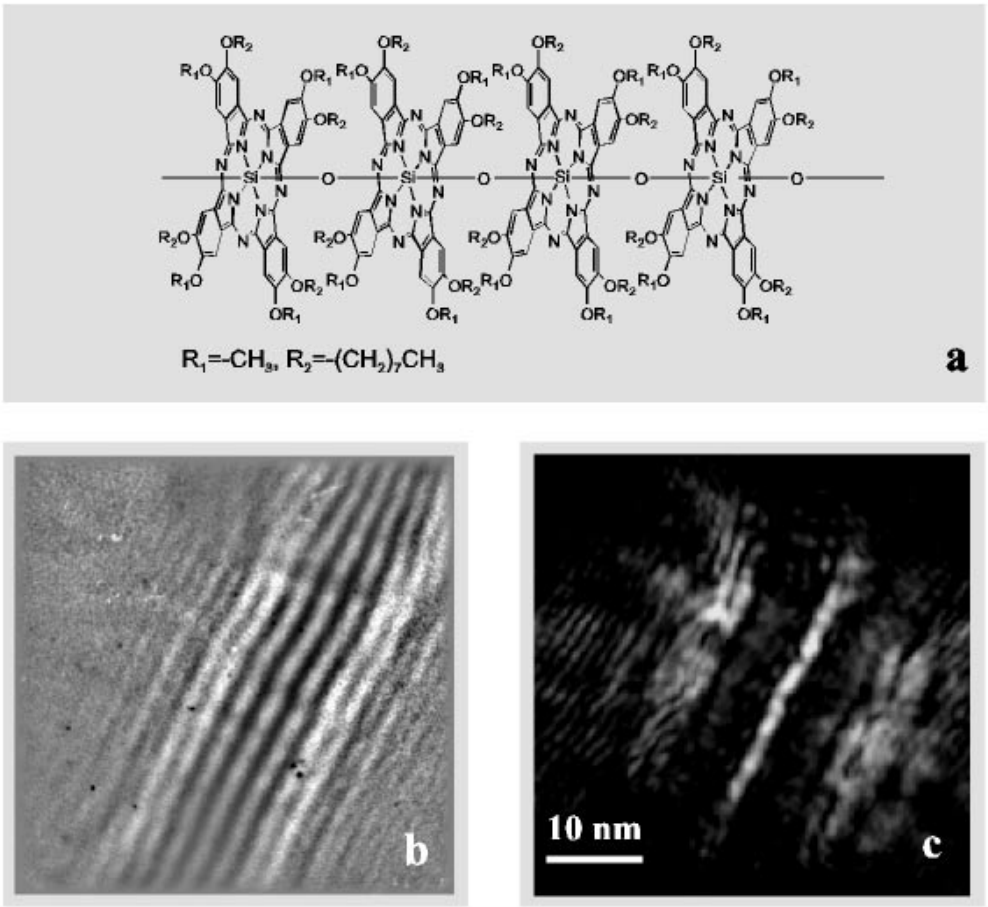

Figure 6. (a) The structure of phthalocyaninato polysiloxane (PcPS). (b) A hologram recorded with a LEEPS microscope: electron energy 71 eV; source–sample distance 200 nm; screen diameter 4 cm; source–screen distance 14 cm. (c) The reconstruction from (b) showing clearly the outline of the molecule; the 'width' of the molecular rod is 2.5 nm. Reproduced from reference [46].

It is worth pointing out at this stage an inherent difference between DIH with electrons and with photons. The Kirchhoff–Helmholtz transform is devised for the reconstruction of holograms resulting from predominantly single-scattering events. This is a good assumption for photons scattering around small objects but less so for low-energy electrons for which materials with heavy atoms have a mean free path considerably less than 100 Å with the result that multiscattering events become increasingly important. The problems associated

with multiple scattering and also with scattering in higher partial waves have been addressed successfully in photoelectron holography and diffuse LEED, and some of the procedures worked out there can be taken over to LEEPS microscopy. On the other hand, macromolecules composed mainly of light elements with small amounts of heavy elements should be ideal objects for LEEPS microscopy.

As with DIH with photons, the analysis of the LEEPS holograms requires three issues to be addressed:

(1) The detailed physical mechanism by which the images are formed.
(2) How can the three-dimensional reconstruction of the wavefront at the object be achieved.
(3) Under which experimental conditions can we obtain the maximum information about the object?

To address the first issue we developed a theory to simulate LEEPS microscope images [11], and for the second we can use the same algorithm for the numerical reconstruction of the wavefront at the object [12] as was used in optical DIH. The third question has been addressed in a recent paper concerned with the optimization of the LEEPS microscope for the imaging of macromolecules [46]. To provide tools to delineate the range of applicability of the LEEPS microscope and to optimize its operation, a list of operational parameters were examined including electron energy, coherence of the electron beam, angular spread and profile of the electron beam, source–object distance, transparency of the object, size and location of the detector, dynamic range of the detector. Because these parameters are interrelated and interdependent it is crucial to perform an optimization analysis to determine their best choice. It was concluded that intramolecular features in the subnanometre regime can be resolved in LEEPS microscopy with energies around 200 eV, source–object distances of around 0.1 μm, and a screen of about 7 cm diameter, placed 10 cm from the source to yield a magnification around 10^5. The recording should be done with 1024×1024 pixel resolution and a minimum 8-bit dynamic range.

In addition, experimental challenges such as suitable sample preparation, sample mounting, avoiding distortion due to stray magnetic fields and in the accelerating electric field due to the sample holder, and the reduction of electron-induced damage must be addressed in the near future to make LEEPS microscopy a successful endeavour. Much of this has also been discussed in a recent paper where detailed references are provided [46].

In a last remark we address the problem of depth resolution. It has been shown by a combination of simulation and reconstruction that the LEEPS microscope should be capable of atomic resolution and should also be able to distinguish between different atomic types, provided enough data are gathered on a large enough screen [47, 48]. This is particularly true for the lateral resolution but unfortunately less so for depth resolution. For the latter, one finds (in the simulations) not only that atomic 'spots' are smeared out over several atomic diameters but also that there are secondary peaks produced that are spurious and not associated with atomic positions in the object. The problem of poor depth resolution has also been encountered in photoelectron and LEED holography and a remedy has been suggested and successfully implemented using the superposition of reconstructed images for several wavelengths as discussed in other articles in this Special Issue.

References

[1] Gabor D 1948 *Nature* **161** 777
[2] Leith E N and Upatnieks J 1962 *J. Opt. Soc. Am.* **52** 1123
Leith E N and Upatnieks J 1963 *J. Opt. Soc. Am.* **53** 1377
Leith E N and Upatnieks J 1964 *J. Opt. Soc. Am.* **54** 1295

[3] Hariharan P 1996 *Optical Holography* (Cambridge: Cambridge University Press)
[4] Kreis T 1996 *Holographic Interferometry* (Berlin: Akademie)
[5] Aoki Y 1970 *IEEE Trans. Audio Electroacoust.* **18** 258
[6] Kronrod M A, Yaroslavski L P and Merzlyakov N S 1972 *Sov. Phys.–Tech. Phys.* **17** 329
[7] Demetrakopoulos T H and Mittra R 1974 *Appl. Opt.* **13** 665
[8] Onural L and Scott P D 1987 *Opt. Eng.* **26** 1124
[9] Liu G and Scott P D 1987 *J. Opt. Soc. Am.* A **4** 159
[10] Onural L and Oezgen M T 1992 *J. Opt. Soc. Am.* A **9** 252
[11] Kreuzer H J, Nakamura K, Wierzbicki A, Fink H-W and Schmid H 1992 *Ultramicroscopy* **45** 381
[12] Kreuzer H J and Pawlitzek R P 1993–1998 *LEEPS, Version 1.2* A software package for the simulation and reconstruction of low-energy electron point source (LEEPS) images and other holograms
[13] Schmid H, Fink H-W and Kreuzer H J 1995 *J. Vac. Sci. Technol.* B **13** 2428
[14] Kreuzer H J, Fink H-W, Schmid H and Bonev S 1995 *J. Microsc.* **178** 191
[15] Kreuzer H J 1995 *Micron* **26** 503
[16] Kreuzer H J and Pawlitzek R A 1996 *Simulation and Experiment in Laser Metrology; Proc. Int. Symp. on Laser Applications in Precision Measurements (Balatonfüred, Hungary, 3–6 June 1996)* ed Z Füzessy, W Jüptner and W Osten (Berlin: Akademie)
[17] Kreuzer H J and Pawlitzek R A 1997 *Fringe '97: Proc. 3rd Int. Workshop on Automatic Processing of Fringe Patterns (Bremen, Germany, 15–17 September 1997)* ed W Jüptner and W Osten (Berlin: Akademie)
[18] Kreuzer H J, Pomerleau N, Blagrave K and Jericho M H 1999 *Proc. SPIE* **3744** 65
[19] Xu W, Jericho M H, Meinertzhagen I A and Kreuzer H J 2001 *Proc. Natl Acad. Sci. USA* **98** 11 301
[20] Gabor D 1949 *Proc. R. Soc.* A **197** 454
[21] Barton J J 1988 *Phys. Rev. Lett.* **61** 1356
[22] Heinz K, Starke U and Bernardt J 2000 *Prog. Surf. Sci.* **64** 163
[23] Barton J J 1991 *Phys. Rev. Lett.* **67** 3106
[24] DeVelis J B, Parrent G and Thompson B J 1966 *J. Opt. Soc. Am.* **56** 423
[25] Singfield K L, Xu W, Jericho M J and Kreuzer H J 2001 in preparation
[26] Haine M E and Mulvey T 1952 *J. Opt. Soc. Am.* **42** 763
[27] Hanszen K J 1982 *Adv. Electron. Electron Phys.* **59** 1
[28] Lichte H 1986 *Ultramicroscopy* **20** 293
[29] Tonomura A 1987 *Rev. Mod. Phys.* **59** 639
[30] Tonomura A, Allard L F, Pozzi D C, Joy D C and Ono Y A 1995 (ed) *Electron Holography* (Amsterdam: Elsevier Science)
[31] Morton G A and Ramberg E G 1939 *Phys. Rev.* **56** 705
[32] Fink H-W, Stocker W and Schmid H 1990 *Phys. Rev. Lett.* **65** 1204
[33] Stocker W, Fink H-W and Morin R 1989 *Ultramicroscopy* **31** 379
[34] Morin R, Gargani A and Bel F 1990 *Microsc. Microanal. Microstruct.* **1** 289
[35] Fink H-W 1986 *IBM J. Res. Dev.* **30** 460
[36] Fink H-W 1988 *Phys. Scr.* **38** 260
[37] Morin R and Fink H-W 1994 *Appl. Phys. Lett.* **65** 2362
[38] Degiovanni A and Morin R 1994 *Proc. ICEM 13, Electron Microscopy 1994* vol 1 (Paris: Les Editions de Physique)
[39] Horch S and Morin R 1993 *J. Appl. Phys.* **74** 3652
[40] Fink H-W, Schmid H, Kreuzer H J and Wierzbicki A 1991 *Phys. Rev. Lett.* **67** 15
[41] Fink H W, Schmid H and Kreuzer H J 1995 *Electron Holography* ed A Tonomura, L F Allard, D C Pozzi, D C Joy, and Y A Ono (Amsterdam: Elsevier Science)
[42] Fink H-W, Schmid H, Ermentraut E and Schulz T 1997 *J. Opt. Soc. Am.* A **14** 2168
[43] Gölzhäuser A, Völkel B, Jäger B, Zharnikov M, Kreuzer H J and Grunze M M 1998 *J. Vac. Sci. Technol.* A **16** 3025
[44] Spence J C H 1997 *Micron* **28** 101
[45] Binh V T and Semet V 1998 *Ultramicroscopy* **73** 107
[46] Gölzhäuser A, Völkel B, Grunze B and Kreuzer H J 2001 *Micron* at press
[47] Kreuzer H J 1993 *Atomic-Scale Imaging of Surfaces and Interfaces* ed D K Biegelsen, D J Smith and S Y Tong (Pittsburgh, PA: Materials Research Society)
[48] Kreuzer H J, Wierzbicki A, Crawford M G A and Roald C B 1993 *Nanosources and Manipulation of Atoms under High Fields and Temperatures: Applications* ed V T Binh, N Garcia and K Dransfeld (Dordrecht: Kluwer Academic)